



Aalborg Universitet

AALBORG UNIVERSITY
DENMARK

The effects of wind-driven rain on the hygrothermal conditions behind wooden beam ends and at the interfaces between internal insulation and existing solid masonry

Hansen, Tessa Kvist; Bjarløv, Søren Peter; Peuhkuri, Ruut Hannele

Published in:
Energy and Buildings

DOI (link to publication from Publisher):
[10.1016/j.enbuild.2019.05.020](https://doi.org/10.1016/j.enbuild.2019.05.020)

Creative Commons License
CC BY-NC-ND 4.0

Publication date:
2019

Document Version
Accepted author manuscript, peer reviewed version

[Link to publication from Aalborg University](#)

Citation for published version (APA):

Hansen, T. K., Bjarløv, S. P., & Peuhkuri, R. H. (2019). The effects of wind-driven rain on the hygrothermal conditions behind wooden beam ends and at the interfaces between internal insulation and existing solid masonry. *Energy and Buildings*, 196(1 August), 255-268. <https://doi.org/10.1016/j.enbuild.2019.05.020>

General rights

Copyright and moral rights for the publications made accessible in the public portal are retained by the authors and/or other copyright owners and it is a condition of accessing publications that users recognise and abide by the legal requirements associated with these rights.

- Users may download and print one copy of any publication from the public portal for the purpose of private study or research.
- You may not further distribute the material or use it for any profit-making activity or commercial gain
- You may freely distribute the URL identifying the publication in the public portal -

Take down policy

If you believe that this document breaches copyright please contact us at vbn@aub.aau.dk providing details, and we will remove access to the work immediately and investigate your claim.

The effects of wind-driven rain on the hygrothermal conditions behind wooden beam ends and at the interfaces between internal insulation and existing solid masonry

Tessa Kvist Hansen^{a*}, Søren Peter Bjarløv^a, Ruut Peuhkuri^b

^aDepartment of Civil Engineering, Technical University of Denmark, Brovej 118, 2800 Kgs. Lyngby, Denmark

^bDanish Building Research Institute, Aalborg University, Denmark, A.C. Meyers Vænge 15, 2450 Copenhagen, Denmark

*Corresponding Author: Tessa Kvist Hansen, tekhan@byg.dtu.dk / tkh@sbi.aau.dk, +45 99402292

Abstract

An inevitable measure when energy retrofitting historic buildings in Europe, is the reduction of building envelope heat loss. On preservation-worthy facades where external insulation is not an option, installation of internal insulation is gaining pace. The historic buildings in Denmark are often constructed with solid masonry facades and wooden decks. The internal insulation may, however, entail potential hygrothermal risks in walls and embedded wood. Measures such as vapour barriers and capillary active insulation materials are continuously evolving and the subject of much current research. The hygrothermal conditions are of great importance for the durability of the building constructions, and for the health and wellbeing of occupants. Wind-driven rain (WDR) is a central factor contributing to water penetration and moisture loads of the exterior walls. Numerous studies have shown that WDR loads influence the moisture conditions in masonry walls and embedded wooden beams, and can even affect interior relative humidity. In the present paper WDR loads on existing façades in a cold temperate climate were determined by measurements and compared to a semi-empirical model. Simultaneously, the hygrothermal conditions within internally insulated walls with exposed brick and embedded wooden beams were monitored. Furthermore, numerical simulations were implemented for clarification of WDR impact. Hygrothermal simulations and previous studies, inevitably show that high WDR loads result in higher moisture content behind the interior insulation. Results from the field measurements of WDR however, cannot directly be referred to the moisture content measured in walls behind interior insulation or beam ends. However, fluctuations in external air humidity

proved to be influential on conditions in the construction. Implementation of a semi-empirical model for calculations of WDR agreed with previous studies in predictions being too conservative when compared to measured WDR.

Keywords: wind-driven rain, internal insulation, hygrothermal performance, moisture transport, in situ measurements

1 Introduction

The purpose of the present study was to investigate the moisture distribution in the façade after actual wind-driven rain (WDR) loads and possibly establish a correlation between WDR and unacceptable moisture conditions in an internally insulated façade of exposed brick. The coherence was investigated, by comparison between hygrothermal conditions in the construction, and measured WDR loads. The aim was also to quantify the real WDR loads on a façade experimentally with in situ mounted WDR gauges, and to identify the impact of this WDR on the moisture content in the masonry wall by monitoring conditions behind the internal insulation as well as at the beam ends. Furthermore, a theoretical semi-empirical model for WDR quantification was implemented to study the reliability of the model, and numerical simulation models were investigated with regard to actual measurements in order to establish the effect of rain intensity.

In Denmark, more than 30% of residential buildings were constructed prior to 1950 [1], most of which are of traditional building style with masonry walls and embedded wooden beams. As WDR has shown to be potentially detrimental in combination with internal insulation, and as internal insulation is becoming more and more of interest with regard to energy savings, the study appears to be relevant, not only for the Danish building sector, but relevant for similar European climates and historic buildings of masonry. The present study includes two test buildings with different locations in Denmark; both are of solid masonry, and are internally insulated. Furthermore, the annual precipitation in Denmark appears to be rising despite varying years, and nationwide the annual precipitation has increased with 100mm since the 1870s (The Danish Meteorological Institute).

Wind-driven rain is rain that passes through a vertical plane in the atmosphere due to the simultaneous occurrence of wind and rain. WDR is generally assumed to be one of the most important factors that must be taken into account in hygrothermal assessments of external vertical structures, particularly with porous building materials such as brick and mortar. WDR is the most influential factor contributing to the wetting and water penetration of external façades, which in turn affects not only hygrothermal properties and durability [2], but also has been shown to influence indoor climate, energy consumption and the risk of mould growth [3]. Internal insulation is vital in energy retrofits of historic buildings where external changes are unacceptable. Unfortunately, interior insulation increases the risk of interstitial condensation,

due to the altered temperature gradient. The lower temperature also reduces the drying potential of the walls. WDR penetrates porous building materials due to pressure and capillary forces. Furthermore, other climatic loads may influence the effect of WDR on hygrothermal conditions in a construction; e.g. radiation may drive the moisture to further penetration, or the ambient RH that influences due to the hygroscopic properties of masonry seeking equilibrium with surroundings. Capillary migration of WDR contributes to moisture induced risks within internally insulated masonry, especially where vapour barriers, capillary inactive insulation materials [4], or diffusion tight paint on the interior surface are present, as they make it more difficult for the moisture to evaporate inwards. Thus the effect of WDR on historic masonry with applied internal insulation is of high relevance. Damaged façades are less resistant to WDR and therefore internal insulation should only be installed on intact façades. Damaged or weathered bricks, joints and render should be replaced or repaired before internally insulating [5][6]. Mould or wood decaying fungi growth in embedded wood are not the only risks associated with the accumulation of moisture in the masonry façade. The risks also include a resulting decrease in durability due to frost damage, surface soiling, and salt migrations [7], not to mention the reduced thermal resistance caused by an accumulation of moisture (especially for capillary active insulation systems) [8].

Basic moisture transport mechanisms in and around an internally insulated solid wall with embedded wooden beams are illustrated in Figure 1. The figure omits the possibility of air flow behind insulation plates in the event of air pockets, and around the beam ends. The moisture transport mechanisms include vapour diffusion due to vapour pressure differences between internal and external conditions. Through porous building materials capillary suction is the migration of liquid moisture, whether it is present due to condensation, WDR, or rising damp. In other words, capillary suction is the driving force of moisture transport in saturated pores, whilst at lower humidities within the pores the main transport mechanism is diffusion. Convective moisture transport occurs as a consequence of damp air moving through leakages, etc. At thermal bridges, e.g. partition walls and floor slabs, the colder surface temperature also makes it possible for moisture to accumulate.

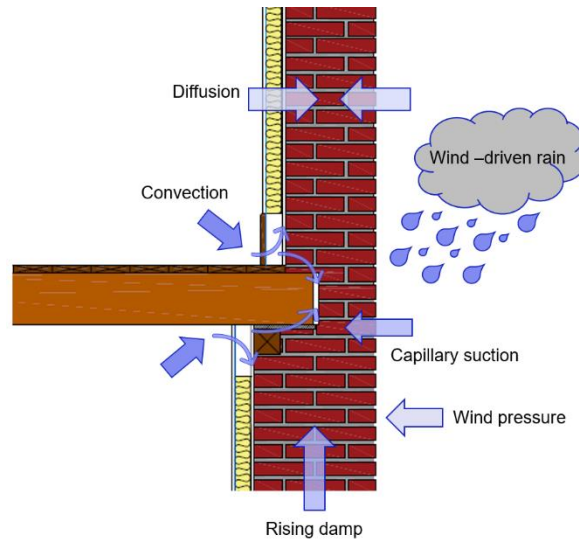


Figure 1: Typical moisture transport mechanisms in an internally insulated wall

The magnitude of WDR is a function of rain intensity, size and distribution of raindrops, and wind speed. The simultaneous occurrence of wind and vertical rain generates WDR, which can be referred to as a sloped vector [2], illustrated in Figure 2. The terminal velocity of the raindrop is dependent on the size of the raindrop; larger droplets fall faster [9], but are less easily carried by wind [10]. The impact on the façade is affected by additional factors, such as 1) building geometry, 2) local topography, 3) climate conditions, including air temperature, air relative humidity, wind conditions, duration of rain, solar radiation, and 4) façade condition.. Studies have shown that the edges [11] and top of a building are most exposed to WDR provided there is no existing roof overhang [12]. This phenomenon can be partly explained by the varying wind pattern across an obstacle such as a building, and the fact that the edges are subjected to WDR from two sides. The wetting of edges has also proved to be more prolonged when compared to central areas of the facades, due to the lower temperatures and reduced drying potential [3]. Masonry consists of porous building materials, bricks and mortar, which are capable of moisture movement. Thus by capillary forces, moisture may migrate to internal locations of a construction provided there is no barrier or cavities. Furthermore, strong solar loads may drive moisture from large WDR loads further into the construction [13].

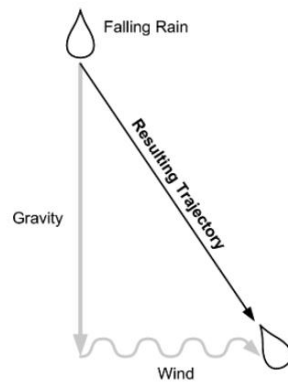


Figure 2: Basic illustration of wind-driven rain [9].

There are three methods for WDR quantification, namely experimental quantification by measurements, numerical simulations models, and semi-empirical models [2][14]. The present work includes experimental methods as well as implementation of semi-empirical and numerical models based on climate data.

Experimental quantification of WDR loads is not a standardized procedure, although it is always performed with a WDR gauge. Wall-mounted WDR gauges have been implemented in experimental work since the 1930's and a variety of designs have been used. The designs vary in shape, size, materials, whether or not they are recessed in the wall, and whether or not they are installed with automatic wipers; variations that have been found to yield discrepancies [2]. The most influential source of error in connection with WDR measurements has been identified as the evaporation of adhered water on the collector plate. Other sources of error include splashing of rain drops, evaporative losses from the reservoir and connecting tube, condensation on the collection area and wind errors. A deeply recessed WDR gauge type has proven to reduce the splashing errors with high wind speed and rain intensity, while in the case of light rain, the large collection area generated large evaporative losses, and splashing in this case was irrelevant [2][14]. The condensation error on the collector surface has been estimated in simulations [14], and shown to be small. This is the only error source that can increase measured results, which are thus liberal.

Numerical models of WDR are based on computational fluid dynamics. WDR is often implemented in numerical simulations as boundary conditions, and thus dependent on climate input. Abuku et al. performed extensive research on WDR, comparing measurements and numerical simulations [15][16]. A test building was set up for WDR measurements in actual climate conditions. The test building included specially installed test sections for monitoring WDR, weight changes in specimens, surface temperature, and runoff water for monitoring the moisture response to WDR impact. Large differences were detected between measurements and simulation results. The differences could not all be attributed to the

convective moisture transfer coefficient, β_e , used in the HAM simulations. A parameter study of β_e as a function of the reference wind measured did show some influence on results and compatibility. The discrepancies found were also attributed to various error sources such as adhesion, evaporation, splashing, bouncing, and spatial and temporal averaging of rain drops. For these reasons, the penetration of rain water may not always be as effective as assumed by some models, why reduction factors are included. The fact that many of the parameters interact, makes it is very difficult to make precise numerical simulations of WDR with single influential parameters (rain, wind, RH etc). Niklewski et al. however, managed to predict the moisture content in rain exposed wood by applying a boundary conditions with elevated moisture concentration during rain events [17], while a similar success was achieved by Dohnal et al. by omitting rain data in simulations, and increasing RH to 100% during rain events. Both Niklewski and Dohnal's studies were specified for wood.

Several semi-empirical calculation models for WDR have been developed, and they are continuously under development and improvement. They are all based on the theoretical formula expressed in Eq. 1, where r_{WDR} represents rainfall intensity for WDR and r_h unobstructed horizontal rain [l/m^2], $U(z)$ the wind speed [m/s] at height z [m] and V_t the raindrop terminal velocity of fall [m/s].

$$\text{Wind-driven rain} \quad [l/m] \quad r_{WDR} = r_h \cdot \frac{U(z)}{V_t} \quad (\text{Eq. 1})$$

The terminal velocity of raindrops depends on the size of the droplets [18]. The size of raindrops varies even in the same rain event, and thus a median value for rain drop size can be implemented. The median rain drop diameter is determined by Eq. 2 [19];

$$\text{Median rain drop diameter} \quad [mm] \quad \bar{d} = 1.105 \cdot r_h^{0.232} \quad (\text{Eq. 2})$$

In 1972 Dingle and Lee [20] managed to define a simplified relation between raindrop size and the terminal velocity in still air with good agreement for droplets in the range of $0.3 \leq \bar{d} \leq 5.88mm$. This relation was also described by Straube [21] and Blocken and Carmeliet [19]. Thus the terminal fallspeed can be expressed as in Eq. 3;

$$\text{Terminal velocity of} \quad [m/s] \quad V_t = -0.166033 + 4.91844 \cdot d - 0.888016 \cdot d^2 + 0.054888 \cdot d^3 \quad (\text{Eq. 3})$$

raindrop in still air

The wind speed at height z [m] is calculated by Eq. 4, and takes the exposure due to terrain and surroundings into account by means of the exponent α [-], as defined by Straube [9]. U_{10} represents wind speed [m/s] at a height of 10 m, as from standard weather stations.

$$\text{Wind velocity at height } z \quad [m/s] \quad U(z) = U_{10} \cdot \left(\frac{z}{10}\right)^\alpha \quad (\text{Eq. 4})$$

In 1955 Hoppestad introduced the WDR coefficient DRF [2][19], which is a proportionality constant between rain on a vertical and horizontal plane, given as $\frac{1}{v_t}$. In 1965 Lacy refined the formula in Eq. 1 to Eq. 5, including the DRF. DRF is empirically defined in the range of 0.2-0.25 for average rainfall intensity, however it has been found to range from 0.15 (intense cloudbursts) to 0.5 (drizzle). Therefore, DRF is variable depending on the rain intensity, and a variable DRF has also been included in this study.

$$\text{Wind-driven rain} \quad [l/m^2] \quad r_{WDR} = DRF \cdot U(z) \cdot r_h \quad (\text{Eq. 5})$$

For estimation of rain deposition on a building, Lacy suggests additions to the WDR calculation as seen in Eq. 6, in order to account for location on the building, as well as wind direction.

$$\text{WDR deposition on facade} \quad [l/m^2] \quad r_{bv} = DRF \cdot U(z) \cdot r_h \cdot RAF \cdot \cos(\theta) \quad (\text{Eq. 6})$$

In Eq. 6 θ is the angle between the normal to the wall and the wind direction. RAF is the rain admittance function. RAF varies from <0.20 below a roof overhang to >1 at the top and edges of high-rise ($>10m$) buildings without roof overhang, as seen in Figure 3 [19][9].

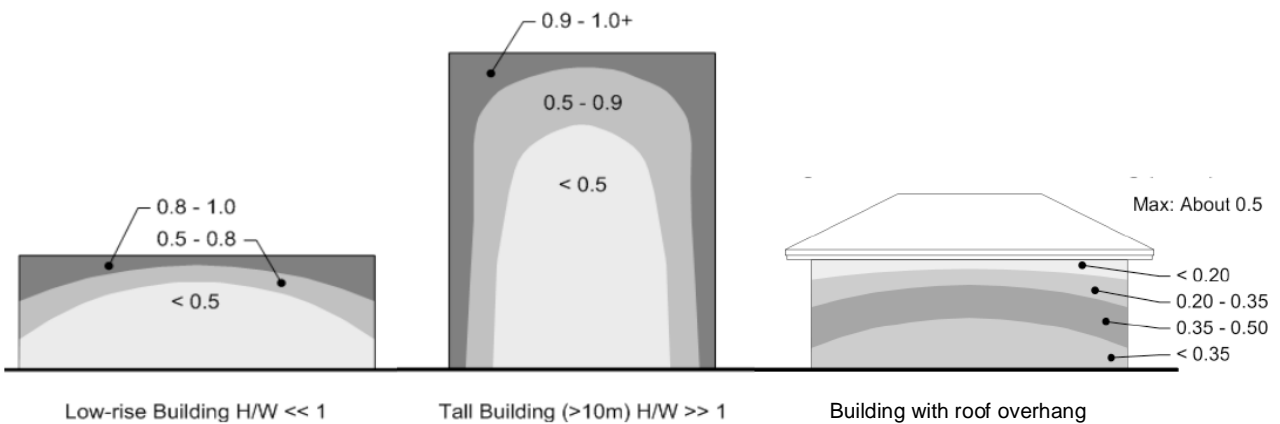


Figure 3: Rain admittance function, RAF, on areas of building facades for low-rise, high-rise and buildings with roof overhang [9].

Morelli et al. [22] compiled a short review of studies on masonry walls with wooden beams. Most of the reviewed literature stated that WDR was not problematic as long as the façade was intact (no cracks or degraded joints). These studies did not clearly reference WDR loads or climate conditions, and WDR was not included in the hygrothermal simulations. Morelli et al. also studied potential moisture risks at beam ends in masonry walls subjected to WDR. The study was based on FMEA (Failure Mode and Effect Analysis) and hygrothermal simulations of retrofitted masonry walls with embedded wooden beams as story-partitions, and internal insulation. The hygrothermal simulations with WDR with various intensities did not show any sign of an effect on the moisture conditions behind the insulation, but with high rain intensity the beam ends could exceed critical moisture content (threshold value for wood with regard to rot/deay is 95-85% RH at 0-30°C [23], threshold for masonry with regard to frost damage varies significantly between brick types [24] however RH above 80% may initiate mould growth [25]). For medium rain load (RAF value of 0.3) it was seen that in cases with free air flow around the beam (20 mm to three sides) and reduced insulation (omitting 200 mm insulation above and below the beam), the moisture content had a tendency to be lower than in constructions with full insulation, which tended to increase the moisture content. Simulations with vapour barriers applied to the case with reduced insulation indicated no impact on the drying potential of beam ends, so the 20 mm air gap around the beam is the influential factor. It was concluded that WDR had a substantial impact on the moisture conditions in beam ends, and that the rain intensity was a very influential factor.

D'ayala et al. performed a similar study on moisture dynamics in two historic buildings with monitored WDR. With regard to semi-empirical WDR models, they established the significance of the climate data – implementation of on-site wind and rain measurements yielded good estimates with regard to cumulative WDR when compared to climate data from the closest weather station, that significantly underestimated the gauge measurements [26].

Abuku et al. investigated the interaction between indoor and outdoor climate, and a solid masonry building envelope with a focus on WDR impact on hygrothermal response, including mould growth, indoor climate and energy consumption. Using numerical simulations, the hygrothermal conditions in the brick wall and room were determined. The study found a distinct impact of WDR on the humidity of internal wall surfaces and indoor humidity. Critical periods were seen especially in summer and winter, and the walls were especially affected in the south and west wall-orientations, as this is also the dominant wind direction at the location of the study [3]. A subsequent study by Abuku et al. compared WDR field measurements with numerical simulations, and determined the responses of the walls to WDR loads. The study indicated that predicted WDR loads were often overestimated in numerical modelling of moisture content, partly because of the splashing of raindrops hitting the wall surface not being considered in standard HAM modelling, and partly due to

averaging errors in absorption and evaporation [16]. Klõšeiko et al. reported a study of field measurements of four different internal insulation systems. They found a certain impact from exterior conditions/rain as increased humidity was measured at the interface between insulation and brick in the case of a vapour tight insulation material [27]. A study by Vereecken et al. on capillary active interior insulation systems demonstrated that driving rain influenced hygrothermal behaviour undesirably [8]. The study investigated whether a capillary active solution performed better than a vapour tight system on single leaf, exposed external masonry wall constructions with a dynamic indoor environment. Adding (large) WDR loads in numerical simulations resulted in high relative humidity on the interior side of the masonry in both insulation systems, and of the reference wall. The relative humidity in the case of vapour tight insulation reached roughly 100 % for the entire year, whereas the capillary active system illustrated the capability for inward moisture transport and drying potential when the drying to the exterior occurred slowly at low temperatures. With regard to moisture accumulation after WDR loads, the vapour tight system showed slower drying; only external drying could occur in this case. In the case of capillary active insulation and a reference wall without insulation, it was seen that WDR loads also influenced the relative humidity on the interior wall surface. This study also found that at high WDR loads, the thickness of the masonry wall had an impact on the masonry moisture content regardless of insulation type, and on the indoor relative humidity in cases of capillary active insulation.

2 Methods and experimental setup

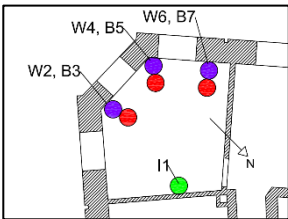

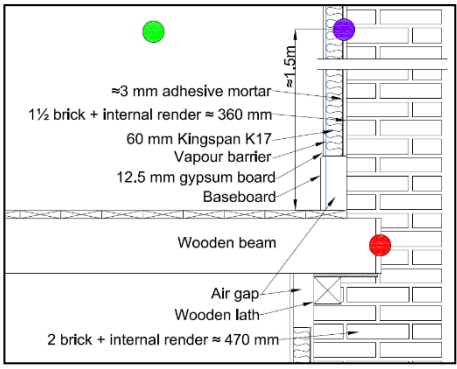
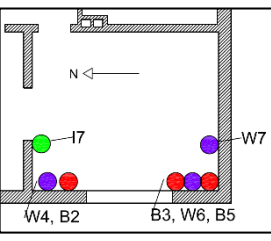

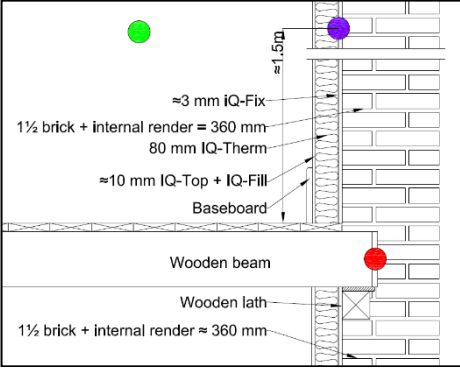
In order to identify the possible water ingress from WDR, gauges measuring WDR and sensors monitoring the hygrothermal conditions within the masonry wall (at wall-insulation interfaces and behind beam ends) were installed on two test buildings in Denmark.

2.1 Test Buildings

The test buildings were two multi-story buildings of typical Danish masonry construction (1850-1950) with embedded wooden beams between the stories. Danish constructions from this time are assumedly constructed with lime mortar, however renovations may have occurred and weathered joints may have been replaced by a cementitious mortar. Both buildings had retained their original construction, with 350 mm solid bare brick external walls at the top floor, which was investigated. Table 1 shows the construction after internal insulation had been applied. The differences included the insulation material and its thickness as well as the thickness of the masonry below each story partition and the elevation of the insulated wall. In addition, the major difference between the two buildings is the fact that the insulation system in test building 1 comprises of phenolic foam boards, with integrated vapour barrier and plaster board. This system was

installed with 20 cm air gaps above and below the beam to create intentional thermal bridges and thus warmer conditions and better drying potential at the beam ends. It should be noted, that despite the integrated vapour barrier, the system has previously shown not to be diffusion tight [28]. The insulation system in test building 2 was installed all the way to the beam, with no air gaps. The system itself comprises of PUR foam boards made capillary active with calcium silicate channels in a grid of 40x40 mm. The thermal conductivities of the two systems are 0.020 W/mK and 0.037 W/mK for test building 1 and 2 respectively. The respective U-values were estimated based on the same brick type, and are displayed in Table 1. In situ measurements were performed behind the internal insulation and beam ends in both test buildings, as marked on the illustrations in Table 1.

Table 1: The two test buildings, sensor locations, façade images and section view of insulated façade. The (numbered) dots represent locations for outputs; purple represents sensors placed at the interface between existing wall and internal insulation (W); red represents measurements behind the beam end (B); green represents the sensor monitoring indoor climate (I). In both cases one measurement is made for interior conditions and three measurements behind both beam ends and insulation.

Test building 1: <i>Meinungsgade, Copenhagen, East Denmark</i>		
<p>From 1877 story building 5th floor Residential SW façade Retrofit: Dec. 2014</p> <p>U-values before / after renovation: 1.24 W/m²K / 0.26 W/m²K</p>	 	
Test building 2: <i>Ny Allégade, Haderslev, South west Denmark</i>		
<p>From 1932 3 story building 2nd floor Residential W façade Retrofit Jan. 2015</p> <p>U-values before / after renovation: 1.24 W/m²K / 0.33 W/m²K</p>	 	

2.2 Inspection of façades

Before installing WDR measuring equipment, the façades of the test buildings were examined in order to identify potential surface defects which could influence the results. The façades of both test buildings were inspected visually, as cracks,

high moisture content, frost damage, salt efflorescence or other abnormalities could influence WDR penetration [13] or hygrothermal conditions. Furthermore, the sorptivity of the façade bricks, and mortar joints in test building 2, were estimated by Karsten tube [29], in order to identify possible significant differences in the water absorption capabilities.

2.3 Climate data

Climate data was gathered from local weather stations from the Danish Meteorological Institute (DMI). DMI weather stations do not all collect the same data, which is why the data is spread out on several weather stations, as provided in Table 2. The weather data implemented in the present study was chosen to be from weather stations closest to the test building location. Table 2 indicates the distance between the weather station and test building, and the data is considered adequate for this study.

Table 2: Climate data and origin.

Case	Climate data	Weather station no.	Distance from test building
Test building 1	Precipitation	5725	1.7 km
In situ WDR measurements: 24/06-16 – 11/01-17	Temperature, relative humidity, wind velocity, wind direction, cloud cover	6180	3 km
	Global radiation	6187	10.5 km
Test building 2	Precipitation	5390	0.9 km
In situ WDR measurements: 07/06-16 – 10/01-18	Temperature, relative humidity, wind velocity, wind direction, cloud cover	6110	12.5 km
	Global radiation	6123	24.4 km

The climate data was used for WDR calculations with the semi-empirical approach, to compare these to the WDR gauge measurements for validation and estimation of the rain admittance function theoretically. Furthermore the climate data was implemented in the simulations models, by producing .ccd climate files with 1 hour time steps. The climate files in Delphin are used for generation of boundary conditions (heat conduction, vapour diffusion, short and long wave radiation and driving rain) in the hygrothermal modelling of test building 1. Similarly, the indoor climate (temperature and relative humidity) measured in the test building was included in the dynamic simulation.

2.4 Wind-driven rain gauge

The WDR gauge designed for the experiment was based on existing types, experience and comparative tests. It was based on the gauges manufactured at K.U. Leuven's Laboratory for Building Physics, with some alterations according to recommendations found in the literature. The area of the collection plate was 300x300 mm, with a 10 mm raised rim around all the edges. The raised rim caught splashing water to some extent [16], and prevented collection of water from

outside the collection area [14][30]. The plate was constructed in acrylic glass (PMMA), which has shown better performance and fewer errors due to water adhesion/evaporation in comparison with teflon (PTFE) [2]. The WDR was monitored by a HOBO Rain Gauge (Metric) Data logger, which was a closed tipping bucket rain gauge that minimizes the evaporation losses from the reservoir. The data logger was fixed to the collection plate, and the water drained directly into the HOBO. The HOBO had a diameter of approximately $\text{\O}15$ cm, which meant that the collector plate was extended out slightly from the wall surface. The WDR gauge is illustrated in Figure 4. The gauge is also described in [31,32] It was set to monitor rain events, and calibrated prior to use. The calibration showed that one counted rain event corresponded to 3.78 ml and 3.72 ml for test buildings 1 and 2 respectively.

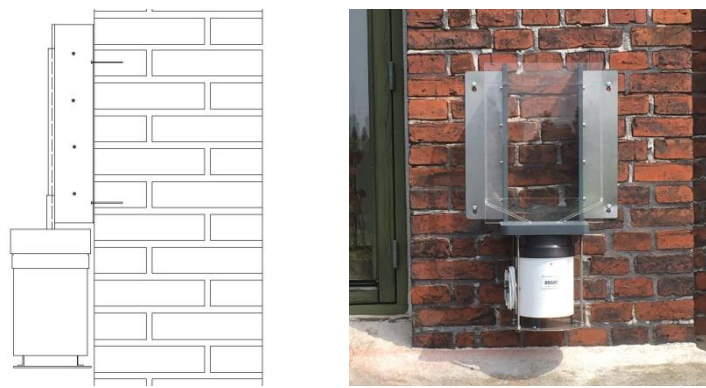


Figure 4: Wall-mounted WDR gauge with HOBO logger. Illustration (left) shows fixation and extension from surface. Image (right) illustrates fixation to façade (test building 1)

As indicated in Table 1, the WDR gauge on test building 1 was mounted on the SW façade, at the 5th floor height. This faces a large cemetery, so no buildings or obstructions in the direct vicinity were expected to influence the WDR measurements. On test building 2, the WDR gauge was located on the W façade at 2nd floor height. This facade was facing the street. The distance to the closest neighbor in this direction was approximately 20 m and there were no large trees or other obstructions in the immediate vicinity.

2.5 WDR calculations

WDR deposition on the façade was estimated by Eq. 6, described in the introduction, as it accounts for the wall orientation by including cosine of the wind directions angle to a normal of the wall, and furthermore accounts for the location on a façade. A variable DRF value has been implemented as dependent on the rain intensity and varying median rain drop diameter, and thus terminal fall speed of raindrops. The height implemented in the calculations represented the heights in which the WDR gauges were installed; 14 m for test building 1, and 5 m for test building 2. For calculation of wind speed at the respective heights, the exposure exponent α was estimated to be 0.3 for test building 1 (between suburban and city

center conditions) and 0.25 for test building 2 (suburban). The RAF value was estimated based on the measured values, and a RAF value of 0.2, according to Figure 3 was also implemented. The climate data used for the semi-empirical calculations was, as stated in section 2.3, taken from the closest weather stations, but due to the distances some discrepancies can be expected. Temperature and relative humidity sensors

Temperature and relative humidity sensors were placed behind the internal insulation and behind the beam ends, as marked on the illustrations in Table 1. As seen on the floor plans, three measurements behind the beam ends, three measurements behind the insulation, and one measurement of interior conditions were performed in both cases. Rotronics HygroClip2 HC2-S were used and built into the construction before installing the insulation. Sensors behind the insulation were placed in existing joints or in purposely designed indentations. Sensors behind the beam ends were placed in holes drilled from the inside. The holes were subsequently filled with insulation and sealants to avoid any external influence on the measurements. The temperature and humidity conditions in the interior environment were also monitored with similar equipment. The data was logged every minute, and connected directly to an online service for transmitting the data. The data was later converted into hourly averages.

Determination of material parameters for the existing materials in the test buildings was not included in the present study, so the calculations of moisture content were based on material properties and sorption isotherms of lime plaster and spruce, for wall-insulation interfaces and beam ends respectively. Basis for material selection were based on the lime plaster being included in validated simulations [28], and thus it was used as interface material, and spruce was chosen as one of three wooden materials in the database which did not differ significantly from each other. The sorption isotherms were defined by the Delphin material database, and can be seen in Figure 5. Under the assumption of instant moisture equilibrium between material and air, the sorption isotherms of lime plaster and spruce were implemented for determination of moisture content in the measuring points at wall-insulation interfaces and beam ends.

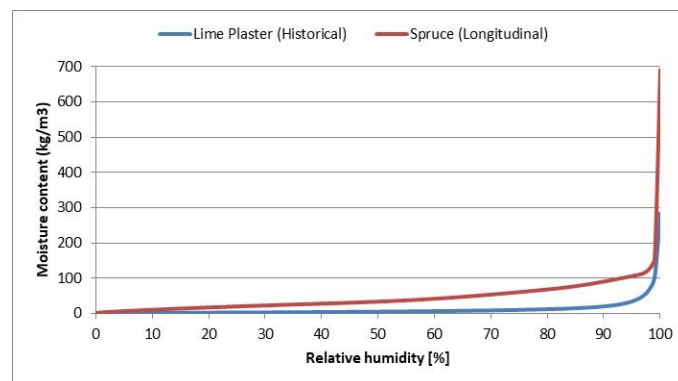


Figure 5: Sorption isotherms of lime plaster and spruce, defined by the Delphin material database. Experiments performed at Technical University of Dresden at 20-23°C.

The gathered data for temperature and relative humidity in the indoor and external climate, were converted to absolute humidity. The absolute humidity, or water vapour content, is calculated by means of temperature, and vapour pressure based on the measured relative humidity [33,34].

2.6 Hygrothermal simulations

In order to further investigate the effect of WDR on hygrothermal conditions in internally insulated masonry, numerical simulation in Delphin [35] was performed. Delphin bases its WDR modelling on an existing numerical simulation technique, and includes building geometry and climatic data, and experimental validation by Bert Blocken and Jan Carmeliet [36]. Delphin uses CFD-simulation for determination of catch ratios for various zones on the building envelope for steady state wind flow patterns by a 4 step technique. Furthermore, the rain drop size distribution is determined based on measurements from a large number of rain events, determined by Best [37]. The difference between the raindrop size distribution in the air and through a horizontal plane, is accounted for by inclusion of the terminal velocity of rain drop falls, defined by Gunn and Kinzer [35]. The method resulted in catch ratio tables, from which Delphin defines catch ratios by linear interpolation, and thus the rain load normal to the wall surface as a function of time can be defined. The absorption of rain water by the façade is dependent on the degree of saturation and material parameters. Thus the numerical models are able to quantify the WDR effect, and with various values of RAF, and thus possibly contribute to support the experimental findings. A simplified approach of WDR modelling on case buildings, was constructed with 1D models based on the validated model of test building 1, described in [28]. The 1D models account for less influential factors than a 2D model, however the 1D approach was found suitable for this purpose. The climate data gathered from the weather stations described in section 2.3 was implemented in the models. The simulation models were set to quantify the relative humidity and temperature at the wall-insulation interface. RAF=0.2 was used as best estimate for model validation. To further investigate the importance of RAF, further models were calculated with RAF=0, RAF=0.4, RAF=0.6, RAF=0.8, and RAF 1. The results of RH were transformed into moisture content based on sorption isotherms like the measured data, as described in section 0.

3 Results and discussion

3.1 Façade conditions

The façades were inspected in connection with the installation of WDR measuring equipment, in June 2016 for both cases. The visual inspection revealed significant differences in the masonry of the two test buildings. Images of the masonry can be seen in Figure 6. Test building 1, from 1877, appears to be significantly weathered and several cracks are apparent when compared to test building 2. Furthermore, test building 1 exhibits many signs of masonry renovation and repairs, as several mortar types are visually apparent. Test building 1 is 55 years older than test building 2, and located directly adjacent to a central traffic route in the heart of Denmark's capital, Copenhagen. It is reasonable to assume that the concentration of the city's air pollution, and the building's age, have contributed to the deterioration apparent in the façade. In test building 2, from 1932, the masonry appears much more intact, and only a few minor damages are apparent. The Karsten tube measurements did not reveal any significant differences in the estimated sorptivities of the two brick types. The sorptivity of the mortar joints in test building 2 was found to be more than 2.5 times larger than in the two brick types. This was expected, as the mortar joints are assumed to be of lime mortar in Danish historic masonry. A previous study on moisture transport properties in brick [38] also showed a higher sorptivity on a lime mortar rendered brick specimen compared to a brick specimen that was not rendered. The results from the mortar joints in test building 2, however, yield the possibility of WDR penetration in mortar joints being dominant.



Figure 6: Masonry on façades of test building 1 (left) and test building 2 (right)

3.2 Climate data, WDR calculations and WDR measurements

The number of rain events found in climate data for each wind direction (N, NE, E, SE, S, SW, W, NW), are illustrated in Figure 7 alongside the average wind-driven rain in the respective wind direction for each location of test building. The

average WDR was calculated based on Eq. 1, thus without the inclusion of the orientation and is considered the general WDR.

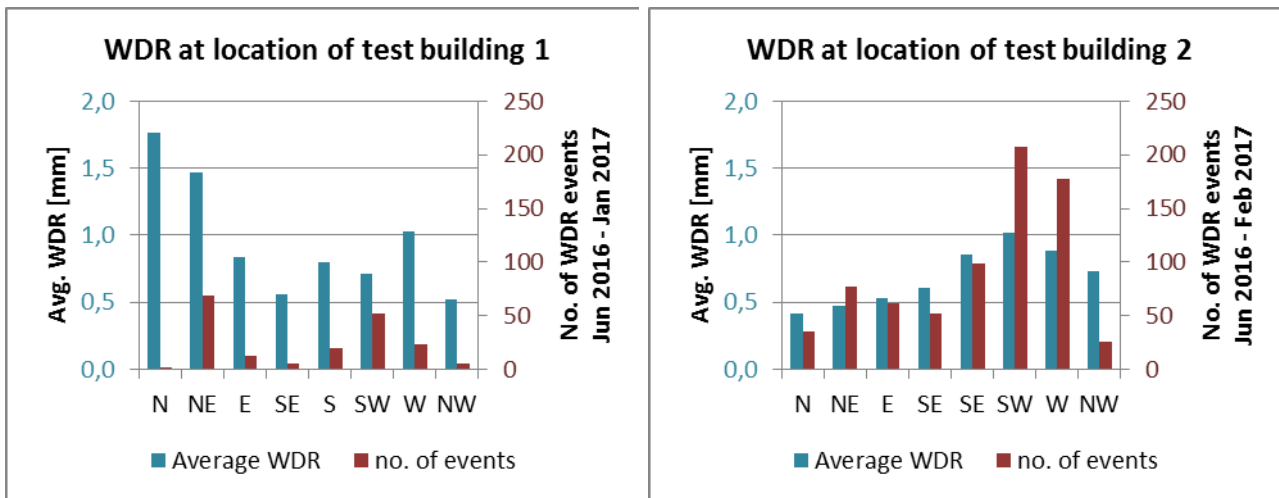


Figure 7: Number of rain events counted for the given period and wind directions (red), and the average WDR for events in this wind direction (blue).

As seen in Figure 7, the wind patterns between the two case buildings vary significantly. The results from test building 1 indicate varying wind patterns, and the results appear more random when compared to test building 2. The wind measurements applied for test building 1, were from near the coast, which could influence the wind patterns. For test building 1, it appears that WDR from NE is dominant, as both the frequency and intensity in the given time period are the highest. The rest of the data from test building 1 resembles the data from test building 2, with high frequency and magnitude of WDR, from South, Southwest, and West directions. This is also considered the orientation where the highest amount of WDR will hit a vertical facade in Denmark. As the orientation of the test buildings are SW and W for test building 1 and 2 respectively, they are considered worst case scenarios in terms of WDR load.

Calculations of deposited WDR were performed on the basis of Eq. 6 in the introduction, thus based on the climatic data of wind speed, wind direction, and unobstructed horizontal rain, as well as consideration to building height, and variable terminal velocity of raindrops, and thus a variable DRF. As it can be seen from Figure 8, the value of DRF is well in accordance with previously found and empirically estimates values. For both test buildings, the average value of DRF was found to be 0.27, and in the range of [0.15;0.32].

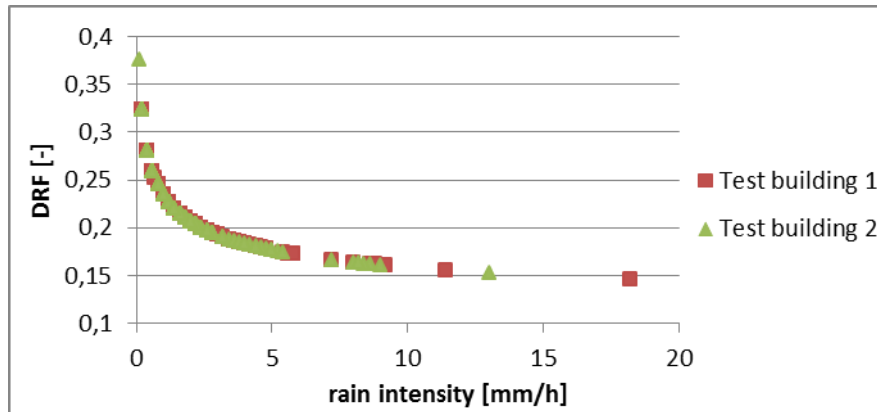


Figure 8: Variable DRF found from climate data from the two test sites

The implementation of the semi-empirical WDR model was performed in two ways. Initially, the RAF value was set to 0.2 in accordance with Figure 3. Secondly, the RAF value was adjusted according to the measured WDR data. This generated RAF values of 0.065 and 0.1 for test building 1 and 2 respectively. Results of the cumulative WDR from both calculations and the measurements are presented in Figure 9. The measured WDR was based on event counts from the tipping gauge, and calibrated against the amount of rain per event for each gauge, and furthermore corrected to be l/m^2 .

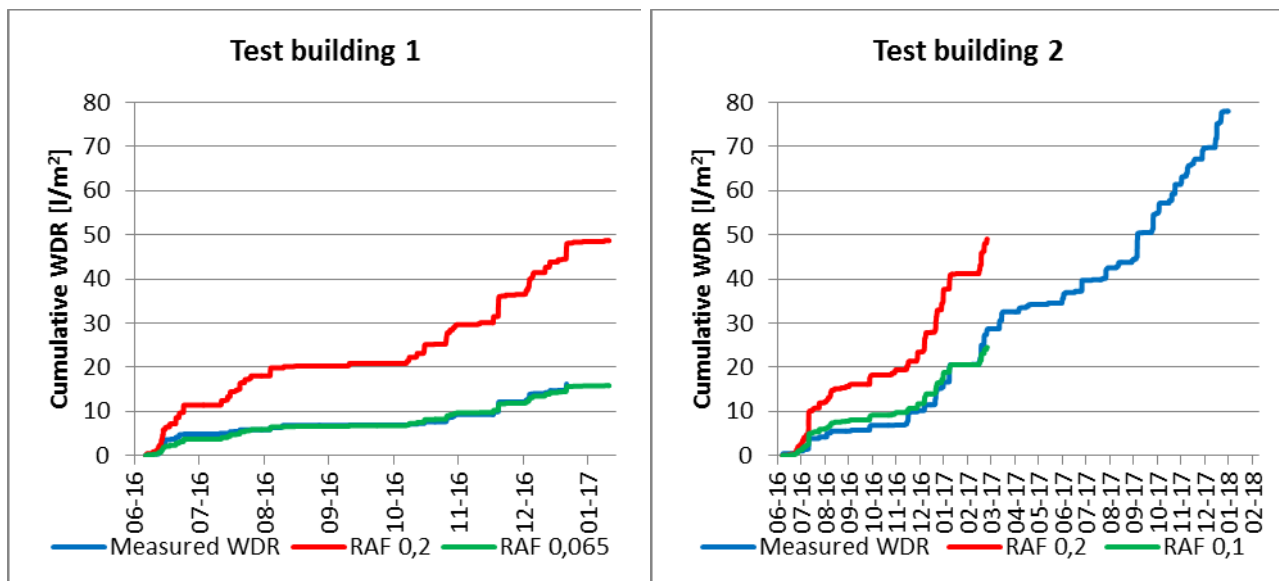


Figure 9: Cumulative WDR based on calculations with two RAF values (red: 0.2 and green: 0.065/0.1) as well as measured data (blue). The bottom axis represents dates in month-year format.

The theoretical calculations of WDR with a fixed RAF value of 0.2 yielded results with similar tendencies as WDR events and dry periods occurred simultaneously for both measured and calculated values. The magnitude of the results however, did not correspond to measured WDR, as the calculated cumulative WDR appeared to increase too steeply. In fact, the theoretical calculations with RAF 0.2 yielded significantly higher results of deposited WDR. For test building 1 the calculated results were 2.5 times larger than the measured; for test building 2 the calculated results were nearly twice the

measured at the end of the studied period. It appears that the model overestimates WDR. Fitting the semi-empirical model to measured WDR values, generated relatively low RAF values that did not correspond to standardized RAF values, as seen in Figure 3. Thus both methods stress the semi-empirical model being too conservative. Some of the discrepancies may however be explained by sources of error connected to the WDR gauge measurements, e.g. adhesion, evaporation and splashing, which were not accounted for in the theoretical calculations [15]. Furthermore, the design of the WDR gauge, protruding from the façade surface, may have caused disturbances in the wind pattern. Finally, the calculations were based on climate data gathered from the closest weather stations and not the exact locations. Especially the wind patterns in a city with tall buildings may vary very locally, influencing the calculation results. Nath et al. [39] performed a study on mid- and high-rise buildings in Canada for the comparison of measurements and theoretical WDR by means of a different WDR model (ISO 15927-3:2009 [12]). In nearly all cases, they similarly found the semi-empirical model to overestimate WDR up to three times the measured values. D’Ayala et al. [26] also found discrepancies between measured WDR and a semi-empirical calculation method – the tendencies were alike, however not the magnitude. By replacing the wind direction and wind velocity from the nearest weather station, to wind measurements performed on site, much better agreement was found. This emphasizes that climate can be very local, why this may influence results significantly. In fact, D’Ayala et al. thus concluded that weather station climate data is insufficient with regard to determinations of exposure of a specific building.

3.3 Hygrothermal conditions in wall and beam ends in relation to WDR

Measured results of relative humidity are presented in Figure 10 and Figure 11, together with measured WDR for test buildings 1 and 2 respectively. The hygrothermal conditions measured behind the beam ends and at the wall-insulation interfaces for the two test buildings were presented and elaborated in previous work by the authors [28]. WDR is portrayed in dark blue, measured conditions in purple and red nuances, for wall-insulation interfaces (W) and beam ends (B) respectively. The external climate is levelled as 36 hour running average, and portrayed in light blue, and the internal conditions in green.

Relative humidity measurements from test building 1 show, that the relative humidity in beam ends is generally higher when compared to the wall-insulation interfaces, with the exception of W6. Initially measurements from W6 mostly resemble beam end conditions. This sensor is located at an indentation of the wall, and thus approximately at the same distance to exterior, as beam end measurements. From the measured relative humidities in test building 1, Figure 10, it is difficult to see a clear impact of WDR on the hygrothermal conditions. E.g. at the end of September 2016, the relative

humidity increased without any occurrence of significant rain events, which indicates that other environmental factors, likely exterior and interior moisture loads, have a more significant influence than WDR. In fact, in the same period, the external RH begins to rise as a natural seasonal variation, and this effect is seen in all sensor measurements. Some peaks in the relative humidity subsequent to rainy spells, e.g. in the beginning of July 2016, are present. But if these and other changes in the hygrothermal conditions within the wall are the result of wind-driven rain, the delay and effect of other climate conditions such as solar radiation, cloud cover and temperature, remain unclear.

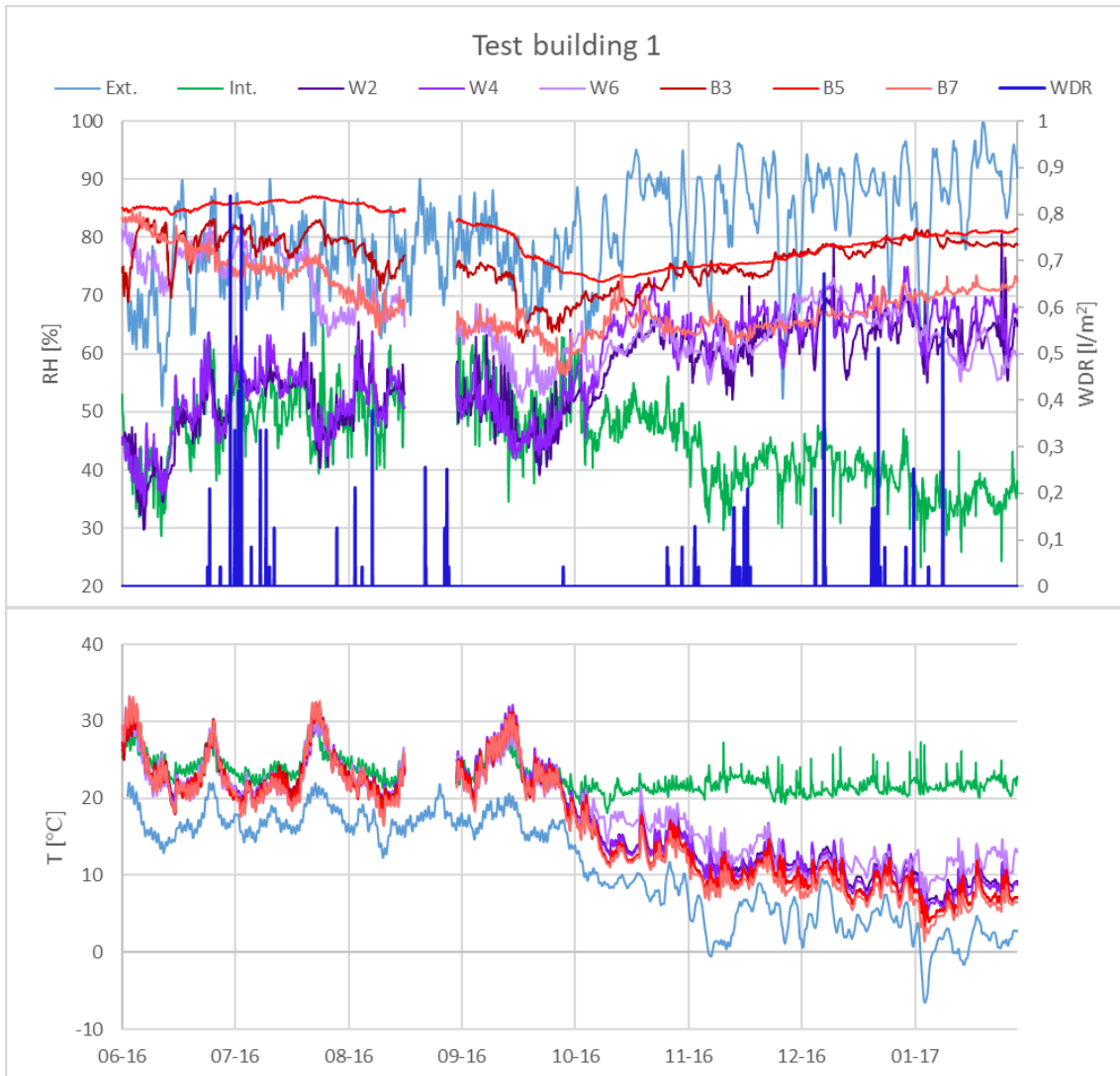


Figure 10: Relative humidities and temperatures measured behind beam ends (red) and at wall-insulation interfaces (purple), as well as measured WDR (dark blue) in test building 1. Furthermore the outdoor (light blue) and indoor (green) conditions are portrayed. The bottom axis represents dates in month-year format.

In test building 2, the monitored relative humidity was extremely high for the duration of measurements, Figure 11. All sensors, with the exception of B2, exhibited relative humidity in the range of 95-100%. Therefore it is impossible to identify any shifts in connection with monitored wind-driven rain in the wall. The measurements from B2 are assumed to be located in the vicinity of a hot water pipe, as the registered temperatures are consequently higher than the rest during

winter, and up to 10°C difference is observed. Sensor B3 does however indicate a slight tendency of seasonal variation with higher RH in winter periods and a slight reduction for summer. These observations indicate the influence of external RH rather than WDR. As the measured relative humidities from this test building are so high, further analysis of this case is discarded. As seen in Figure 7, test building 2 is exposed to up to 4 times as many rain events on the southwest façade, when compared to test building 1. Furthermore, on this façade, the magnitude of the events appear larger. These facts, in conjunction with the large sorptivity in these joints, may suggest an influence from WDR, however it cannot be proven. Furthermore, the sorptivity in the joints of test building 1 was not registered, and may be of the same proportions.

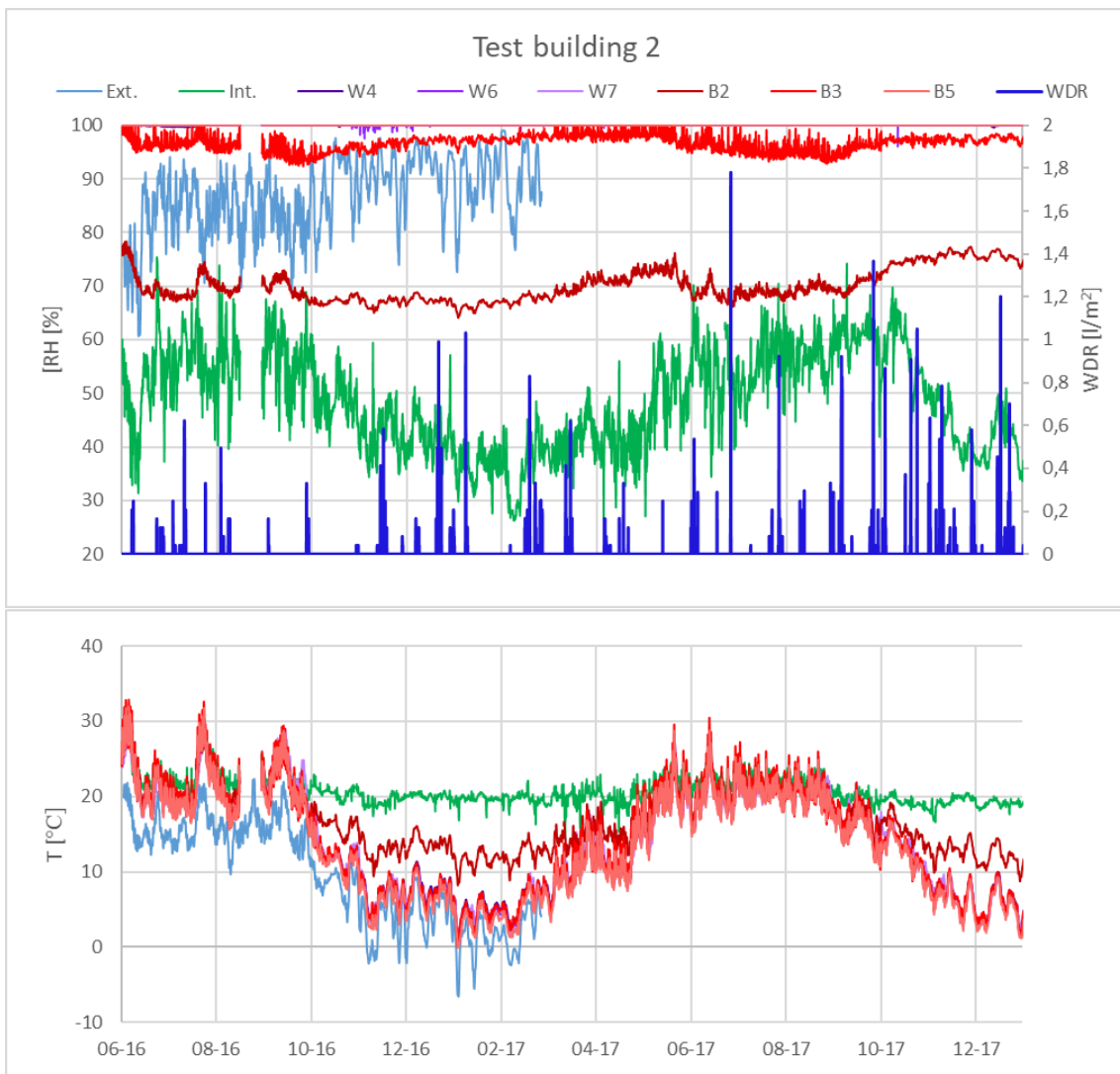


Figure 11: Relative humidities and temperatures measured behind beam ends (red) and at wall-insulation interfaces (purple), as well as measured WDR (dark blue) in test building 2. Furthermore the ourdoor (light blue) and indoor (green) conditions are portrayed. The bottom axis represents dates in month-year format.

The direct measurement results of relative humidity and WDR do not give any clear answers as to whether WDR has a direct impact on the moisture conditions in the wall or behind beam ends. In order to investigate the possible correlations between WDR and the hygrothermal conditions of internally insulated masonry walls, the measured WDR is presented

in diagrams together with the absolute humidity of internal and external conditions, and the moisture content in the interface between the original wall and the thermal insulation (W) (Figure 12) and behind beam ends (B) (Figure 13) in test building 1. The interior absolute humidity is portrayed in green, and the exterior absolute humidity is portrayed in light blue. Dashed orange circles and lines highlight points of interest, elaborated below. Due to the differences in magnitude of the moisture content at the interface and at beam ends respectively, WDR and AH are portrayed on the 1st and 2nd y-axis in the two figures.

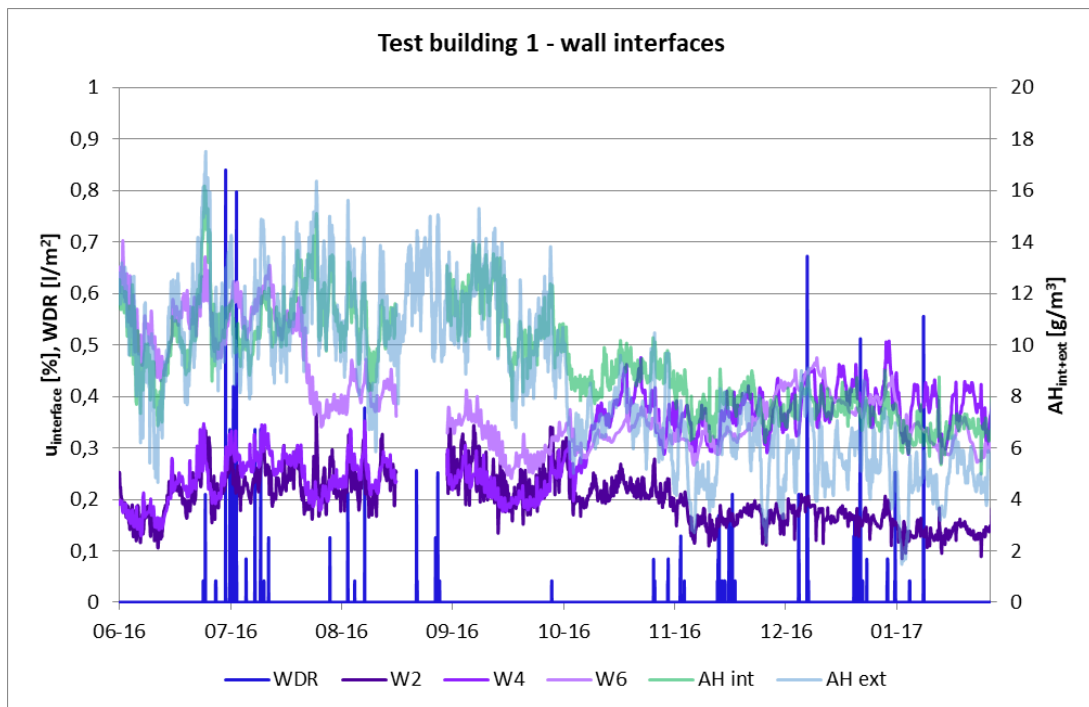


Figure 12: Moisture content in at wall-insulation interfaces, besides internal and external absolute humidity (green and light blue respectively), and measured WDR (dark blue). The bottom axis represents dates in month-year format.

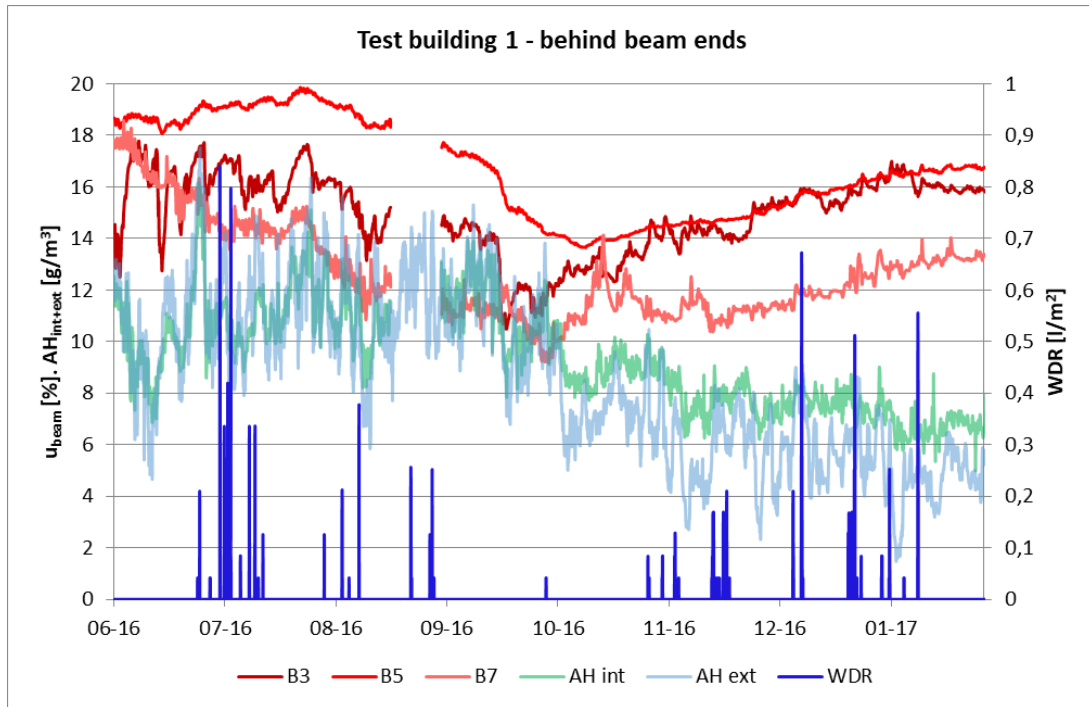


Figure 13: Moisture content in beam ends, besides internal and external absolute humidity (green and light blue respectively), and measured WDR (dark blue). The bottom axis represents dates in month-year format.

In Figure 12 and Figure 13, the direct influence of WDR on hygrothermal conditions is difficult to establish. It can be argued, in some points of time, that peaks in moisture content could be attributed a delayed response to WDR; however this possible influence appears to be insignificant in magnitude. The possible delayed effect of WDR can be observed subsequent to the large rain spell in July 2016, as peaks in W2, W4, W6, and B3 are observed within the following 10 days. The effect is however, inconclusive based on the measurements. On the other hand, when studying the interior and exterior absolute humidities, the impact of these on measurements appear much clearer, and a direct impact can be established in both peaks and tendency. During the summer season, the interior and exterior absolute humidities are very much alike, whereas in the winter season, the interior absolute humidity is higher than the exterior. In the middle of September both interior and exterior absolute humidity drops as a natural seasonal variation, and this is apparent in all the sensor locations as well, as the moisture content also drops. Furthermore, this drop occurs simultaneously with a period of no WDR on that façade. However, the subsequent increase in moisture content also occurs without the influence of WDR, but when the external relative humidity increases. The external absolute humidity is dependent on all rain events, and thus rain events with wind directions not hitting the façade in question, may be partly responsible for the peaks in external humidity. There are several examples of peaks in the internal and/or external absolute humidity that can be transferred to peaks in the moisture content of both interfaces and beam ends. In the beginning of July 2016, there are high peaks in the external absolute humidity, some of which occur simultaneously to large WDR spells on this façade.

These large peaks are visible in the moisture content of nearly all sensors, but primarily for interface measurements. In the middle of August 2016 there are low peaks of internal and external humidity, that are also apparent for moisture content in all sensor locations. There are some examples of the internal absolute humidity peaks independently from the external (e.g. middle of October 2016, middle of January 2017). In these cases, it is seen that the internal moisture conditions have a larger impact on measurements behind beam ends when compared to the effect seen in the interface measurements. This can be attributed to the convection around beam ends, as also portrayed in Figure 1. The external climate appears to be determinative on the indoor climate to some extent. Convection occurs behind the insulation plates as a consequence of grooves in the glue mortar and discontinued vapour barriers. Convection is also possible around the embedded beam end, as there is air around the perimeter. Due to this convection and air flow behind the insulation plates, and around the beam ends, the moist interior air will flow at these points, and thus influence these conditions to a higher extent than the external RH through diffusion.

In winter, it is generally seen that most significant effect from peaks in internal and external absolute humidity is found behind beam ends. At this point, the wall itself is thinner (as the beam is embedded), why the external conditions would reach this measuring point faster than the interface. Moist interior air can also reach the beam ends, as the insulation system with integrated vapour barrier is discontinued 20 cm above and below the floor separation. In the summer, most effect of external/internal absolute humidity is seen at the wall-insulation interfaces. Despite the insulation system having integrated vapour barrier, a previous study [28] has shown the system to allow air flow behind the plates. Due to this phenomenon, moist air can reach the interface.

The time it takes for WDR penetration of 1 or 1½ brick thick masonry was not detectable in the present study. WDR deposit may be redistributed in the wall due to other external factors, e.g. solar radiation, cracks allowing air flow and faster evaporation. Theoretically, if there was a continuous reservoir of water on the façade and perfect contact with the façade and throughout the façade, the penetration of 350 mm of brick (yellow soft molded brick with $A_w = 0.2782 \text{ kg/m}^2\text{s}^{1/2}$ and $\theta_{\text{cap}} = 0.275 \text{ m}^3/\text{m}^3$) would take about 33 hours. According to a partial immersion experiment performed with brick in another study [34], water penetration of 54 mm was apparent after 1 hour in yellow soft molded brick types with full water contact. At this rate, a 1½ brick thick construction would be penetrated in less than 7 hours of full water contact. The above mentioned studies do not include the resistances at e.g. mortar-brick interfaces, why the actual delay of water penetration is assumed higher. Previous studies have found increased humidities due to WDR in cases of vapour tight insulation [8][27], whereas capillary active insulation systems have shown positive results and moisture management [8]. In this case, the insulation system in test building 1 can be regarded diffusion open, as stated in section 2.1. The results

from the numerical simulations are found in Figure 14. Besides the generated moisture content from the simulation results for the interface between the original wall and the thermal insulation for different rain admittance functions (RAF) portrayed in purple nuances, the graph contains measured WDR (blue), internal (pink) and external (light blue) absolute humidity, and lastly results from measurements by sensor W4 (orange). Sensor W4 can be regarded as representative for the interface between the original wall and the internal thermal insulation. Peaks in external moisture conditions, are not only attributed direct WDR events, but also elevated temperatures that increase the moisture capacity of the ambient air, and e.g. other rain events that will not be registered as WDR on the SW façade. In the cases of RAF values of 0.8 and above, the relative humidity exceeds 80% at the end of November and start of December for RAF=1 and RAF=0.8 respectively. At relative humidities above 80%, the moisture content rapidly approaches the maximum in the sorption isotherms, why the curves go beyond the depicted area. The variety in the influence of the rain admittance function (RAF) indeed illustrated the effect of WDR. It is seen, that a RAF of 0 and 0.2 generate very similar results, and that RAF values 0.4, 0.6, 0.8 and 1 appear stacked, and thus the influence of WDR is illustrated in the simulation results. The resulting moisture content behind the insulation increases with increased step in RAF-value, indicating a clear presence and influence of WDR. The results illustrate that the modelled effect of WDR appears larger than the one measured with the WDR gauge, which confirms the overestimations found in semi-empirical models and numerical models (Abuku et al. [15]). The model assumes that all rain, dependent on the RAF value, is absorbed by the masonry, and that all capillaries are in conditions to absorb water, but this water uptake may not be perfect in reality. As the RAF value of 0 generates better results with regard to moisture conditions at the interface, and hygrothermal conditions that appear reasonable, it may be advisable to apply hydrophobization to the external surface in cases of high WDR loads. This may remedy the penetration of moisture, in order to protect the construction.

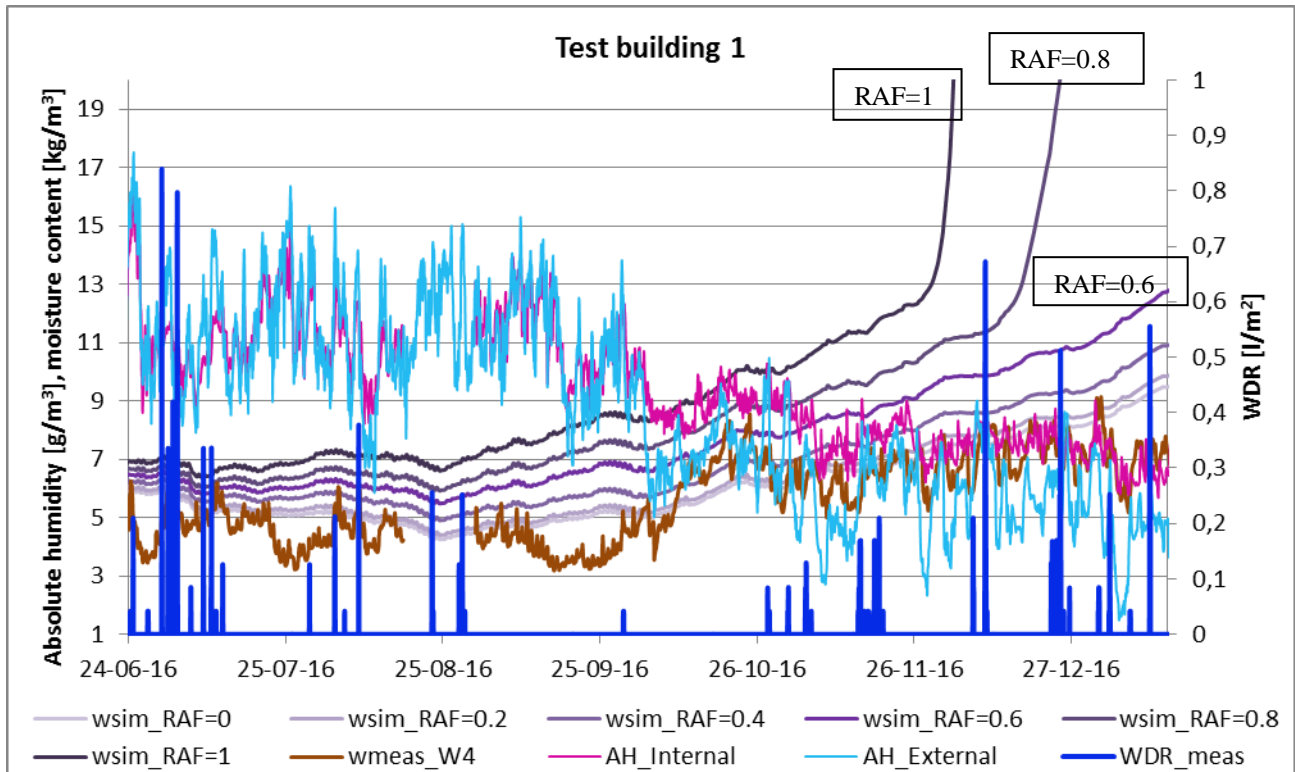


Figure 14: Moisture contents gathered from simulations; *wsim_RAF* stands for moisture content [kg/m³] at the interface between the original wall and the thermal insulation for different rain admittance functions (RAF=[0;1]). Internal and external absolute humidity is also portrayed, as well as the moisture content measured in “W4” and measured WDR

Odgaard et al. [31] found that large rain events, or rain events of longer duration did in fact yield temporary delayed increases in relative humidity during summer seasons. Coelho et al. [40], did a study on solid brick walls of 220 mm, and it was established through simulations that WDR indeed is a main contributor to moisture content in façades. The results from Odgaard et al. yielded delayed and minor, yet visible, increases in relative humidity at the wall plate. In a previous study by the present authors [41], a laboratory study on WDR ingress on internally masonry observed increased relative humidity in the interface between insulation and masonry. The effect however, was delayed. In the interface, the small increase in RH is first detected after 3 24 hour cycles, each with 30 minutes of severe rain, 2 hours of radiation and 21½ hours of cold climate. Smaller increases in RH could even be detected in the internal insulation layer. The results from these studies and the present study indicate the effect of WDR on hygrothermal conditions in internally insulated walls being present, however not necessarily significant. The moisture may be able to dry out somewhat before it penetrates to the wall-insulation interface. In cases where the masonry is thicker, the penetration is delayed further, and the delay allows further drying out. Similarly Vereecken [8] et al. also established the importance of masonry thickness when it comes to WDR protection. Morelli et al. [22,42] did research on WDR based on numerical simulations showing that with high intensity rain events, the beam ends, rather than the wall-insulation interface, were affected by the WDR. Furthermore, Morelli’s study showed the positive effect of the 200 mm air gap above and below the beam. The direct negative effects

of WDR in beam ends were not visible in the present study; they did however generally have higher moisture content than the interfaces, due to material characteristics; parameters and transport mechanisms. Finally, several of the studies referred to [4, 5, 19] stated that deteriorated façades were less resistant to WDR. In the present study, test building 1 had the most deteriorated façade, and furthermore a slightly higher sorptivity. Despite these facts, the monitored effects on the hygrothermal conditions in the masonry were nearly negligible. In a previous laboratory study by the authors [41] on WDR ingress on internally insulated masonry, a clear increase in the relative humidity in the interface between insulation and masonry was observed. The effect however, was delayed. In the interface, the small increase in RH was first detected after three 24 hour cycles, each with 30 minutes of severe rain, 2 hours of radiation and 21½ hours of cold climate. This observation is consistent to the theoretical calculation of penetration time presented above. Smaller increases in RH could even be detected in the internal insulation layer.

4 Conclusion

- The wind-driven rain (WDR) loads have an influence on the moisture conditions in the masonry and behind the applied internal insulation. The direct connection between the measurement of the WDR and the detection of WDR rain events behind the insulation or beam ends was not achieved. A distinct coherence between moisture content and internal and external humidity conditions was however established.
- The research shows that the effect of WDR on internally insulated solid masonry can not only be explained by direct WDR loads and pure capillary transport of this liquid water that highly depends on material parameters. The hygrothermal conditions at the wall-insulation interface are also highly dependent on external moisture conditions, as well as seasonal variations and internal moisture loads. The hygrothermal conditions are also subjected to other factors such as solar radiation and air flow which have not been measured in this study.
- Rain admittance factor (RAF) variations in hygrothermal simulations and previous studies [41] emphasize the importance of the influence of WDR penetration of masonry with regard to hygrothermal conditions in internally insulated walls.
- Semi-empirical models as well as numerical simulations implemented in the present study for quantification of WDR were found to considerably overestimate the WDR load compared to measurements. It appears, that for WDR simulations, diffusion models perform better than fluid dynamics models.

5 Acknowledgements

The work in this paper is a part of project RIBuild “Robust Internal Thermal Insulation of Historic Buildings” that has received funding from the European Union’s Horizon 2020 research and innovation program under grant agreement No 637268. We would like to thank building owners for allowing measurements to be taken. Also acknowledgement for Ph.D. student Tommy Odgaard and LINATEX A/S for collaboration on the development of the WDR gauge, furthermore Tommy for assistance in general WDR analysis.

List of abbreviations

WDR: wind-driven rain [l/m^2]

DRF: WDR coefficient ($1/V_i$)

RAF: Rain admittance function [0;1], [-]

RH: Relative humidity [%]

AH: Absolute humidity [g/m^3]

w: Moisture content [kg/m^3]

6 References

- [1] Statistics Denmark, Byggeri og boligforhold, Stat. Yearb. 2012. (2012) 273–288. <http://www.dst.dk/Site/Dst/Udgivelser/GetPubFile.aspx?id=16252&sid=11byg> (accessed March 27, 2019).
- [2] B. Blocken, J. Carmeliet, A review of wind-driven rain research in building science, *J. Wind Eng. Ind. Aerodyn.* 92 (2004) 1079–1130. doi:10.1016/j.jweia.2004.06.003.
- [3] M. Abuku, H. Janssen, S. Roels, Impact of wind-driven rain on historic brick wall buildings in a moderately cold and humid climate : Numerical analyses of mould growth risk , indoor climate and energy consumption, *Energy Build.* 41 (2009) 101–110. doi:10.1016/j.enbuild.2008.07.011.
- [4] G.R. Finken, S.P. Bjarløv, R.H. Peuhkuri, Effect of façade impregnation on feasibility of capillary active thermal internal insulation for a historic dormitory – A hygrothermal simulation study, *Constr. Build. Mater.* 113 (2016) 202–214. doi:10.1016/j.conbuildmat.2016.03.019.
- [5] G. Christensen, T. Bunch-Nielsen, Indvendig efterisolering af ældre ydermure | BYG-ERFA, BYG-ERFA.

(2009).

- [6] J. Munch-Andersen, SBI-anvisning 221: Efterisolering af etageboliger, 1., Statens Byggeforskningsinstitut, Hørsholm, 2008.
- [7] B. Blocken, M. Abuku, S. Roels, J. Carmeliet, Wind-driven rain on building facades: some perspectives, in: EACWE 5, 2009.
- [8] E. Vereecken, S. Roels, Capillary active interior insulation: do the advantages really offset potential disadvantages?, *Mater. Struct.* 48 (2015) 3009–3021. doi:10.1617/s11527-014-0373-9.
- [9] J. Straube, Simplified Prediction of Driving Rain on Buildings : ASHRAE 160P and WUFI 4.0, *Build. Sci. Dig.* (2010) 1–16.
- [10] E.C.C. Choi, Velocity and Impact Direction of Wind-Driven Rain on Building Faces, *Proc. ICBES'97.* (1997) 465–472.
- [11] H. Ge, R. Krpan, Field measurement of wind-driven rain on a low-rise building in the coastal climate of British Columbia, *Sci. Technol.* (2007).
- [12] DS/EN ISO 15927-3 Hygrothermal performance of buildings - Calculation and presentation of climatic data - Part 3: Calculation of a driving rain index for vertical surfaces from hourly wind and rain data, 2009.
- [13] G. Christensen, A.P. Koch, E.B. Møller, Indvendig efterisolering - ældre ydervægge og murværk, BYG-ERFA. (2015).
- [14] B. Blocken, J. Carmeliet, On the accuracy of wind-driven rain measurements on buildings, *Build. Environ.* 41 (2006) 1798–1810. doi:10.1016/j.buildenv.2005.07.022.
- [15] M. Abuku, B. Blocken, S. Roels, Field measurement and numerical analysis of wind-driven rain absorption and evaporation on building facades, *Building.* 32 (2009).
- [16] M. Abuku, B. Blocken, S. Roels, Moisture response of building facades to wind-driven rain: Field measurements compared with numerical simulations, *J. Wind Eng. Ind. Aerodyn.* 97 (2009) 197–207. doi:10.1016/j.jweia.2009.06.006.

- [17] J. Niklewski, M. Fredriksson, T. Isaksson, Moisture content prediction of rain-exposed wood: Test and evaluation of a simple numerical model for durability applications, *Build. Environ.* 97 (2016) 126–136. doi:10.1016/j.buildenv.2015.11.037.
- [18] N. Sahal, M. a. Lacasse, Water entry function of a hardboard siding-clad wood stud wall, *Build. Environ.* 40 (2005) 1479–1491. doi:10.1016/j.buildenv.2004.11.019.
- [19] B. Blocken, J. Carmeliet, Overview of three state-of-the-art wind-driven rain assessment models and comparison based on model theory, *Build. Environ.* 45 (2010) 691–703. doi:10.1016/j.buildenv.2009.08.007.
- [20] A.N. Dingle, Y. Lee, Terminal fall speed of raindrops_ Dingle and Lee 1972.pdf, *J. Appl. Meteorol.* 11 (1972) 877–879. doi:10.1175/1520-0450(1972)011<0877:TFOR>2.0.CO;2.
- [21] J. Straube, *Moisture Control and Enclosure Wall Systems*, 1998. doi:10.16953/deusbed.74839.
- [22] M. Morelli, S. Svendsen, Investigation of interior post-insulated masonry walls with wooden beam ends, *J. Build. Phys.* 36 (2012) 265–293. doi:10.1177/1744259112447928.[23] J.G. D. Kehl, U. Ruisinger, R. Plagge, Wooden Beam Ends in Masonry with Interior Insulation – A Literature Review and Simulation on Causes and Assessment of Decay, *Proc. 2nd Cent. Eur. Symp. Build. Physics, Vienna 2013* ISBN 978-3-85437-321-6. (2013) 299–304. [http://files/2018/13-09_Kehl_etal_wooden_beam_ends_CESBP2013_ISBN.pdf](http://files/2018/13-09_Kehl_etal_wooden_beam_ends_CESBP2013_ISBN.pdf%5Cnhttps://tu-dresden.de/die_tu_dresden/fakultaeten/fakultaet_architektur/ibk/research/researchprojects/2012_Holzbalkenkoe pfe/13-09_Kehl_etal_wooden_beam_ends_CESBP2013_ISBN.pdf) https://tu-dresden.de/die_tu_dresden/fakultaeten/fakultaet_architektur/ibk/research/researchprojects/2012_Holzbalkenkoe pfe/13-09_Kehl_etal_wooden_beam_ends_CESBP2013_ISBN.pdf.
- [24] P. Mensinga, J. Straube, C. Schumacher, Assessing the freeze-thaw resistance of clay brick for interior insulation retrofit projects, *Proc. Performances Envel. Whole Build.* XI. (2010) 1–8.
- [25] A. Hukka, H. Viitanen, A mathematical model of mould growth on wooden material, *Wood Sci. Technol.* 33 (1999) 475–485. doi:10.1007/s002260050131.
- [26] D. D’Ayala, Y.D. Aktas, Moisture dynamics in the masonry fabric of historic buildings subjected to wind-driven rain and flooding, *Build. Environ.* 104 (2016) 208–220. doi:10.1016/j.buildenv.2016.05.015.
- [27] P. Klõšeiko, E. Arumägi, T. Kalamees, Hygrothermal performance of internally insulated brick wall in cold climate: A case study in a historical school building, *J. Build. Phys.* (2014) 1744259114532609-.

doi:10.1177/1744259114532609.

- [28] T.K. Hansen, S.P. Bjarløv, R.H. Peuhkuri, M. Harrestrup, Long term in situ measurements of hygrothermal conditions at critical points in four cases of internally insulated historic solid masonry walls, *Energy Build.* 172 (2018) 235–248. doi:10.1016/j.enbuild.2018.05.001.
- [29] R. Hendrickx, Using the Karsten tube to estimate water transport parameters of porous building materials, *Mater. Struct.* (2012) 1–12. doi:10.1617/s11527-012-9975-2.
- [30] B. Blocken, *Guidelines for wind, rain and wind-driven rain measurements at test-building sites*, (2004).
- [31] T. Odgaard, S.P. Bjarløv, C. Rode, Influence of hydrophobation and deliberate thermal bridge on hygrothermal conditions of internally insulated historic solid masonry walls with built-in wood, *Energy Build.* 173 (2018) 530–546. doi:10.1016/j.enbuild.2018.05.053.
- [32] Department of Civil Engineering at the Technical University of Denmark, Technische Universität Dresden, Rønby.dk, Ekolab, E&P service, Kingspan, Introflex, Airmaster, COWI, Results and experience from the project: EUDP 2013-II “Energy efficient comfort in older apartment blocks”. Final report, (2016) 203.
- [33] European Standard, *Hygrothermal performance of building components and building elements – Internal surface temperature to avoid critical surface humidity and interstitial condensation – Calculation methods*, Iso 13788. (2013).
- [34] E. Brandt, *SBi-anvisning 224 Fugt i bygninger, 1.*, Statens Byggeforskningsinstitut, Hørsholm, 2009.
- [35] A. Nicolai, J. Grunewald, *Delphin 5 User Manual and Program Reference*, 2006.
- [36] B. Blocken, J. Carmeliet, Spatial and temporal distribution of driving rain on a low-rise building, *Wind Struct. An Int. J.* 5 (2002) 441–462. doi:10.12989/was.2002.5.5.441.
- [37] A.C. Best, Size distribution of raindrops, *Q. J. R. Meteorol. Soc.* 76 (1950) 16–36. doi:10.1002/qj.49707632704.
- [38] T.K. Hansen, S.P. Bjarløv, R. Peuhkuri, Moisture transport properties of brick – comparison of exposed, impregnated and rendered brick, in: *Int. RILEM Conf. Mater. Syst. Struct. Civ. Eng. 2016 Segm. Moisture Mater. Struct.*, Kgs. Lyngby, 2017: pp. 351–360.

- [39] U.K. Deb Nath, V. Chiu, H. Ge, Field measurements of wind-driven rain on mid-and high-rise buildings in three Canadian regions, *Build. Environ.* 116 (2017) 228–245. doi:10.1016/j.buildenv.2017.02.016.
- [40] G.B.A. Coelho, F.M.A. Henriques, Influence of driving rain on the hygrothermal behavior of solid brick walls, *J. Build. Eng.* 7 (2016) 121–132. doi:10.1016/j.job.2016.06.002.
- [41] T.K. Hansen, S.P. Bjarløv, R.H. Peuhkuri, K.K. Hansen, Performance of hydrophobized historic solid masonry - experimental approach, *Constr. Build. Mater.* 188 (2018) 695–708. doi:10.1016/j.conbuildmat.2018.08.145.
- [42] M. Morelli, T.R. Nielsen, G.A. Scheffler, S. Svendsen, Internal Insulation of Masonry Walls with Wooden Floor Beams in Northern Humid Climate, *Therm. Perform. Exter. Envel. Whole Build. XI Int. Conf.* (2010).